Hydraulic fracture visualization by processing ultrasonic transmission waveforms using unsupervised learning A

Aditya Chakravarty[1,1], Siddharth Misra[1,1], and Chandra Shekhar Rai[2,2]

[1]Texas A&M University
[2]University of Oklahoma

November 30, 2022

Abstract

Ultrasonic transmission is sensitive to the variation in mechanical properties of materials. Wave propagation through fractured media introduces changes in the frequency content, travel time and transmission coefficient of the wave. A workflow based on physics-driven unsupervised learning is developed to process the transmitted ultrasonic-shear waveforms to non-invasively visualize the geomechanical alterations due to hydraulic fracturing of a tight sandstone. Novelty of the work involves the assignment of physically consistent clusters to the measurements of shear waveforms across the axial and frontal planes by incorporating the travel time of the peak of spectral energy and transmission coefficient. The proposed workflow generates maps of geomechanical alterations across the frontal and axial planes of the sample. The outputs of the workflow are in good agreement with independent techniques viz. acoustic emission and X-ray computed tomography. The proposed workflow can be adapted for improved fracture characterization in the subsurface when processing sonic-logging, cross-wellbore seismic or surface seismic waveform data.

Hydraulic fracture visualization by processing ultrasonic transmission waveforms using unsupervised learning

Aditya Chakravarty, Dr. Siddharth Misra, and Dr. Chandra S. Rai

For queries contact Dr Sid Misra, Texas A&M University

Abstract — Ultrasonic transmission is sensitive to the variation in mechanical properties of materials. Wave propagation through fractured media introduces changes in the frequency content, travel time and transmission coefficient of the wave. A workflow based on physics-driven unsupervised learning is developed to process the transmitted ultrasonic-shear waveforms to non-invasively visualize the geomechanical alterations due to hydraulic fracturing of a tight sandstone. Novelty of the work involves the assignment of physically consistent clusters to the measurements of shear waveforms across the axial and frontal planes by incorporating the travel time of the peak of spectral energy and transmission coefficient. The proposed workflow generates maps of geomechanical alterations across the frontal and axial planes of the sample. The outputs of the workflow are in good agreement with independent techniques viz. acoustic emission and X-ray computed tomography. The proposed workflow can be adapted for improved fracture characterization in the subsurface when processing sonic-logging, cross-wellbore seismic or surface seismic waveform data.

Introduction

Characterization of mechanical discontinuities (e.g. cracks and fractures) in geological formations, building structural elements (walls, pipes, sheets), composites and metals is crucial for various engineering and scientific pursuits. Geomechanically altered regions are produced due to the propagation of discontinuities and changes in stress. Such geomechanical alterations influence the mechanical properties (e.g. strength, brittleness), storage properties, and transport properties (e.g. fluid, heat). Therefore, it is important to non-invasively visualize the mechanical discontinuities and associated geomechanically altered regions in materials. Machine learning-based workflows are promising methods to process waveforms for the characterization of discontinuities. Our research is an effort to use physics-driven unsupervised learning methods to non-invasively visualize the geomechanical alteration in material by processing multi-point laboratory ultrasonic transmission data.

Various measurement techniques can be used to characterize the mechanical discontinuities at various scales. For example, cross-well seismic survey [1], seismic wave scattering [2], seismic reflections [3], microseismic monitoring [4], and pressure/rate transient analysis [5] are used for fracture characterization at the field scale. Few near-wellbore-scale methods are distributed temperature sensing [6] and micro-resistivity imaging, whereas the laboratory-scale methods include non-destructive acoustic-emission testing [7] and ultrasonic-waveform processing using machine learning [8,9]. For capturing discontinuities at the micro-scale, we can use scanning electron microscopy [10,11].

In this study, multi-point ultrasonic shear-transmission waveforms are processed using physics-driven unsupervised learning to map the spatial variation of geomechanical alteration in materials. Laboratory-scale ultrasonic transmission experiments have been conducted to characterize fracture growth [12], crack density [7], fracture orientation [13] and acoustic emission for localizing damage [10]. Another technique involves displacement discontinuity theory developed based on extensive ultrasonic wave transmission experiments through single/multiple sets of fractures in rocks [14]. Fractures act as low-pass filters explicitly represented through group time delay and transmission coefficient as functions of fracture specific stiffness, frequency, and acoustic impedance of intact medium. Wavelet transform and empirical mode decomposition method can be applied to ultrasonic guided waves to locate flaws in plates [15].

Key advantages of transmission measurements are: (1) minimal interference between the incident and reflected waveforms, and (2) shorter propagation distance allows higher-frequency measurements, at least an order of magnitude higher, that enables better spatial resolution. There are few limitations of transmission measurements, such as (1) higher cost of deployment at the field scale because it is harder to place receivers to acquire the transmission data, (2) reflection data can be interpreted to obtain a three dimensional description, whereas the transmission data can only provide two-dimensional information, and (3) geological materials tend to have a high attenuation coefficient that limits the use of higher frequencies, hence limiting the resolution of transmission measurements.

Method

Experimental setup

The present study analyses the measurements first reported by Bhoumick et al. [7]. Experiments were performed on cylindrical Tennessee sandstone samples having a length of 154 mm and diameter of 152 mm. We define the plane containing the circular face of the sample as the axial plane. The borehole is perpendicular to the axial plane. The planes along the borehole are defined as frontal planes. The experimental parameters and sample details are summarized in Table 1.

Table 1: Experimental parameters

Sample name	TSU6	TSU1
Data	Shear wave transmission Acoustic emission	Shear wave transmission, X-ray CT
Length (mm)	154	154
Diameter (mm)	152	152
Fracturing fluid	Water	Water
Stress (psi)	870	870
Flow rate (cc/min)	15	15
Breakdown pressure (psi)	2764	N.A
Number of located AE	1309	N.A
Injection depth (mm)	80	80
Borehole depth (mm)	83	83
Porosity (%)	9.7	N.A
Permeability (μD)	13	N.A
Composition (wt %)	Quartz 89%, Clay 11%	N.A.

The first step of the measurement is circumferential velocity analysis to determine the P-wave velocity anisotropy and hence the fabric direction in the plane perpendicular to the cylinder axis. In the next step, shear transmission waveforms were measured along the axial and frontal planes using seven source/transmitter and sensor/receiver transducer pairs, arranged in linear geometry as shown in Figure 1. The 1-inch diameter shear transducers are placed 17 mm apart. To ensure firm contact between the sample and transducer, the assembly is pressed on to the sample using air-driven actuators.

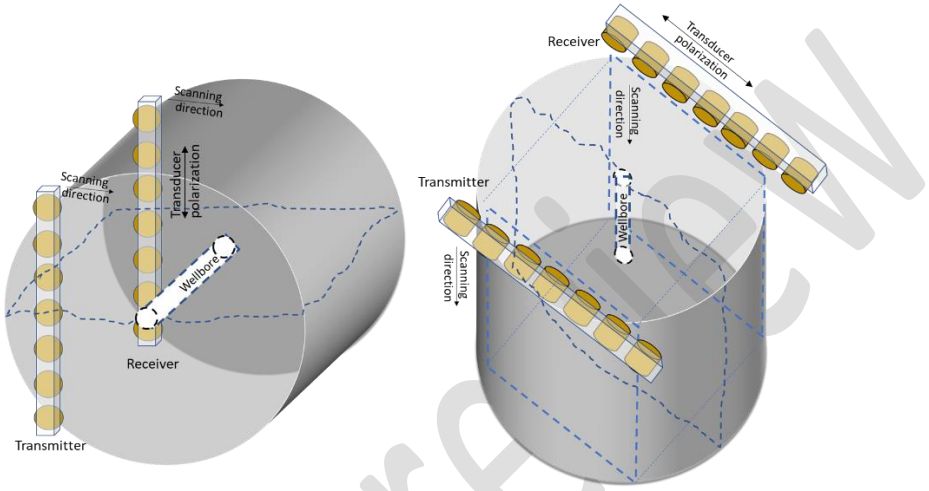

Figure 1: (Top) Schematic of transmitted shear waveform measurements in axial (left) and frontal (right) orientation using 7 pairs of source-receiver transducers. The straight dashed lines in the right-side figure represent the portion of sample cut and removed to create flat surface to facilitate the scanning. The tortuous dashed line in the figures is the anticipated location of the dominant fracture due to hydraulically fracturing.

Prior to the hydraulic fracturing, the transducers are scanned across the axial orientation of the sample (Figure 1, left). Post fracturing, the same scan is repeated. To obtain the shear wave transmission in the frontal orientation, flat surfaces are created on the sample by cutting and removing two portions of the sample 0.5 inches each, from the front and back (Figure 1, right). Consequently, all of the seven transducer pairs are in contact with the sample when scanning in axial orientation, whereas only 5 pairs scan the frontal plane. The bottom plate on which the sample rests is moved at increments of 1 mm for scanning the axial and frontal surfaces, which results in 133 measurement points along each of the two planes (Figure 2). Each transducer assembly (1 source-receiver pair) is active one at a time while recording the shear waveforms. Pre-fracture waveforms are recorded only in the axial orientation, and post-fracture waveforms are recorded for both axial and frontal orientations. Two identical Tennessee sandstone samples, TSU6 and TSU1 were analyzed in our study (refer to Table 1). TSU6 has all the measurements described above, whereas TSU1 does not have the axial ultrasonic transmission and acoustic emission measurements. X-ray computed tomography (CT) measurements were performed only on TSU1.

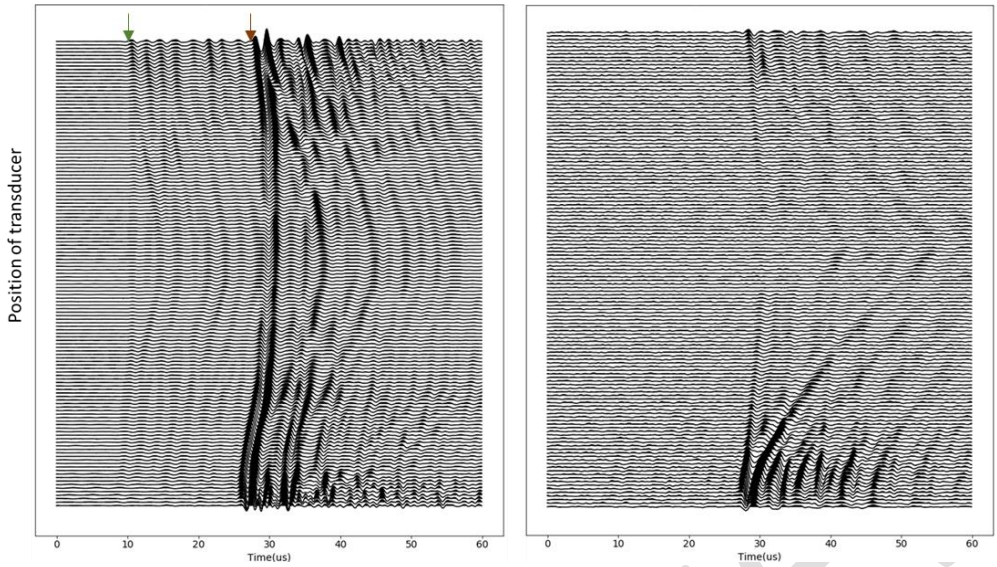

Figure 2: Stack of transmitted waves recorded by Transducer #3 in the axial direction before and after fracture. On the left panel, the green arrow indicates the compressional wave and brown arrow indicates shear wave. Note the drastically reduced amplitudes in the post-fractured case (right). The shear wave 'shadowing' is due to transmission through fractured media.

Unsupervised learning approach

Clustering is unsupervised learning used to detect patterns and hidden structures within a dataset for purposes of grouping the data into clusters. We have considered three methods of clustering: K-Means, Agglomerative and DBSCAN. K-Means clustering is a divisive method that allocates each of the data points to one of the K clusters based on distance between the datapoints and the cluster centroids. The objective of the K-Means cluster-allocation process is to minimize the sum of distances between the cluster centroids and each point in the corresponding cluster to obtain K clusters that have minimum variance around the cluster centroid. Agglomerative clustering initiates the cluster-allocation process by assuming each datapoint as a cluster and then iteratively groups the similar smaller clusters into higher-level larger clusters; this creates a hierarchy of clusters ultimately leading to a single largest cluster containing all the datapoints/samples. This hierarchy of clusters can be visually represented as a dendrogram, which is a tree-like representation showing the similarity between various samples and clusters. The user-specified parameters are distance metric and linkage criteria that govern the agglomerative cluster allocation. Density-based spatial clustering of applications with noise (DBSCAN) assumes that clusters comprise of dense zones in the feature space partitioned by lower density zones. The samples that lie in low-density zones are marked as noise. The user-specified parameters in DBSCAN are the minimum number of neighboring samples and bandwidth that determines the density in the region around each sample.

Feature extraction

Features are categorical/continuous properties/attributes that describe a phenomenon or system that needs to be modeled or investigated using the data-driven methods. Independent, informative and discriminating features are necessary to develop a robust unsupervised learning method. The raw ultrasonic waveform, if used as it is as the feature set, has a very high dimensionality, which is not

conducive to effective clustering. Unsupervised methods perform better on low-dimensional datasets. High dimensionality of the feature set lead to several problems: (1) high computational expense, (2) non-uniqueness of model predictions and solutions, (3) models are not generalizable, (4) increased sensitivity to noise and overfitting, and (5) complicates the interpretation of data-driven models. To reduce the dimensionality of the feature set for purposes of developing well generalizable data-driven models, we deploy short-time Fourier transform (STFT) followed by principal component analysis (PCA) to extract reliable representative features from the waveforms.

The short-time Fourier transform of the waveform yields a spectrogram, which contains the time-frequency content of the waveform. The time-frequency contents are stored as time-varying frequency coefficients. In the present study, each waveform is divided into 12 time-segments, each having 15 frequency bins (Figure 3). Thus, there are 180 STFT coefficients corresponding to each waveform. Principal component analysis (PCA) is applied on the 180 STFT coefficients to obtain a dimensionally reduced feature set. Prior to dimensionality reduction, the features were scaled using Robust scaler. We found that the first two principal components explained 75% of variance exhibited by the STFT coefficients. 76, 65 and 63 PCA derived components explained 98% of variance shown by 180 STFT-derived features for axial, frontal (fracture perpendicular) and frontal (fracture-parallel) orientations, respectively.

From clusters to geomechanical alteration index

Raw clustering results do not convey any physical information because clustering only accounts for statistical relationships and trends. Moreover, raw clustering results are not statistically consistent due to overfitting or underfitting. The clusters are made statistically consistent by finding the optimal cluster number using silhouette score, based on the concept of cohesion and separation. Following that, the clusters are made physically consistent by invoking the displacement-discontinuity theory. A novelty of our work is the use of displacement-discontinuity theory to transform the cluster index to geomechanical alteration index (GAI) to provide certain physical meaning to the clusters. Hence, the treatment makes the clusters statistically and physically consistent.

It is important to define the optimum number of clusters to be identified using clustering methods. This ensures statistical consistency of the clusters. Effective clustering should exhibit low cohesion and high separation. Cohesion is defined as the mean dissimilarity of the data point *i* with all other points in the same cluster. Low cohesion correlates with low intra-cluster distance *a*. Separation is the lowest mean dissimilarity of a data point *i* to other points in the clusters to which the datapoint *i* does not belong [16]. For every data point *i*, the intra-cluster distance is denoted as *a* and the mean nearest cluster distance is denoted as *b* [16]. Then, silhouette score *s* of a datapoint *i* is defined as:

$$s(i) = \frac{b(i) - a(i)}{\max\left(b(i),\, a(i)\right)} \qquad (1)$$

A high silhouette score, i.e. cohesion is low and the separation is high, implies effective clustering [17]. By considering the difference in the median values of the *J* parameter between different clusters and the silhouette scores we determined the optimal number of clusters. The range of J is 0-0.035 for axial and 0-0.01 for frontal orientation, respectively. Large J indicates minimal alteration. Following this, the cluster index are transformed to the geomechancial alteration index. Wave transmission through a fracture results in a reduction of the frequency and energy along with phase change of the wave, as

predicted by the displacement discontinuity model [14]. This results in a delay of the waves' first arrival, and a reduction of the transmitted wave energy (Figure 2 and Figure 3).

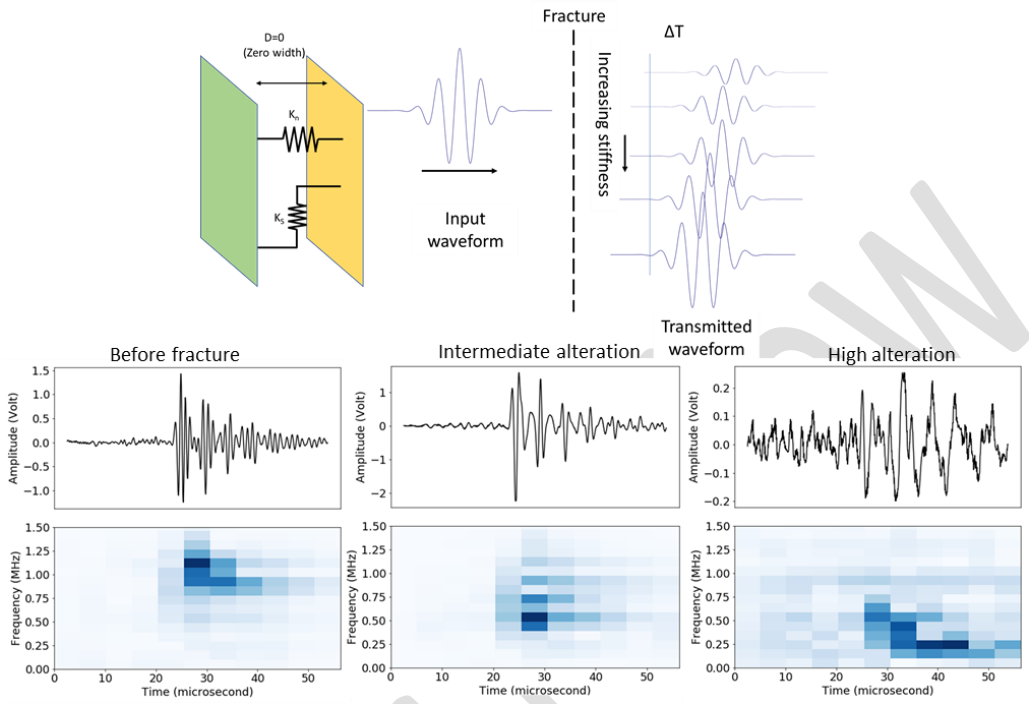

Figure 3: (Top) Schematic diagram of the displacement discontinuity model and the effect of fracture on the transmitted waveforms. (Bottom) Waveforms and corresponding short-time Fourier Transform spectrograms for varying levels of fracture induced alteration. Samples shown are from axial orientation.

The spectral energy density of the transmitted waveform is calculated from the coefficients of the STFT spectrogram. The time of arrival of the first peak of the spectral energy is used as a surrogate for the first arrival of the stress wave. We devise a parameter, *J*, which combines the effects on arrival time and transmission coefficient based on displacement-discontinuity theory:

$$J = \frac{t_c}{t_d} \quad (2)$$

where t_c is transmission coefficient and t_d is arrival time of first peak of spectral energy. Overall the *J* parameter decreases with decreasing fracture specific stiffness, which is a direct indicator of the geomechanical alteration induced by the hydraulic fracturing of the transmission zone. A geomechanical alteration index (GAI) is assigned based on the *J* parameter value. GAI of 1 implies least alteration that correspond to high values of the *J* parameter, and progressively higher GAI indicate higher alteration represented by lower values of the *J* parameter. Without the J parameter, the clusters have no physical meaning. Use of the *J* parameter, assigns the level of damage represented by the cluster. However, we cannot solely use the *J* parameter to assess the damage because it does not consider the entire waveform, whereas the clustering takes the entire waveform into account when grouping the various locations sensed by the shear waveform.

The flowchart to obtain physically consistent geomechanical alteration indices is presented in Figure 4. The transmitted shear wave signals are collected before and after the sample is hydraulically fractured. The extracted STFT of the transmitted shear waveform features are subject to scaling and dimensionality reduction, and then used as input for clustering. To generate the geomechanical alteration indices, the clusters identified using clustering method are first made statistically consistent by using cohesion, separation, and silhouette score to determine optimal number of clusters; following that, the optimal clusters are assigned a physical meaning based on the *J* parameter. results are assigned physical basis by comparing their corresponding transmission coefficient and time of arrival of first spectral peak.

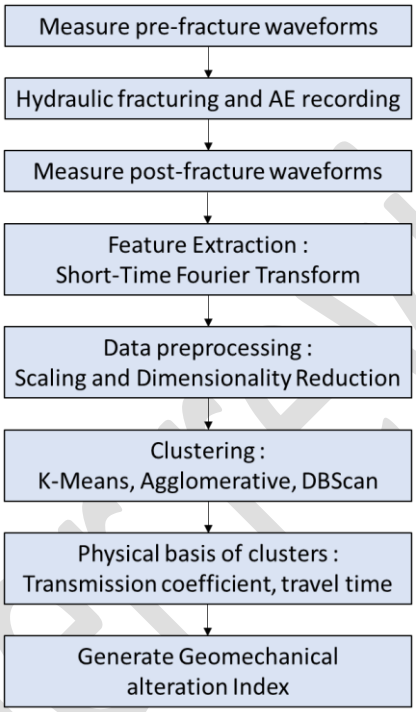

Figure 4: Workflow to quantify the spatial distribution of geomechanical alteration due to fracturing

Results and discussion

Feature extraction

When a wave propagates through a discontinuity, the frequency, temporal, and energy contents of the wave are altered, and these changes are better reflected in the parameters obtained from the short-time Fourier transform (STFT) of the waveform. This is evidenced by the partition of STFT derived waveform features of intact and fractured data projected in principal component space as shown in Figure 5.

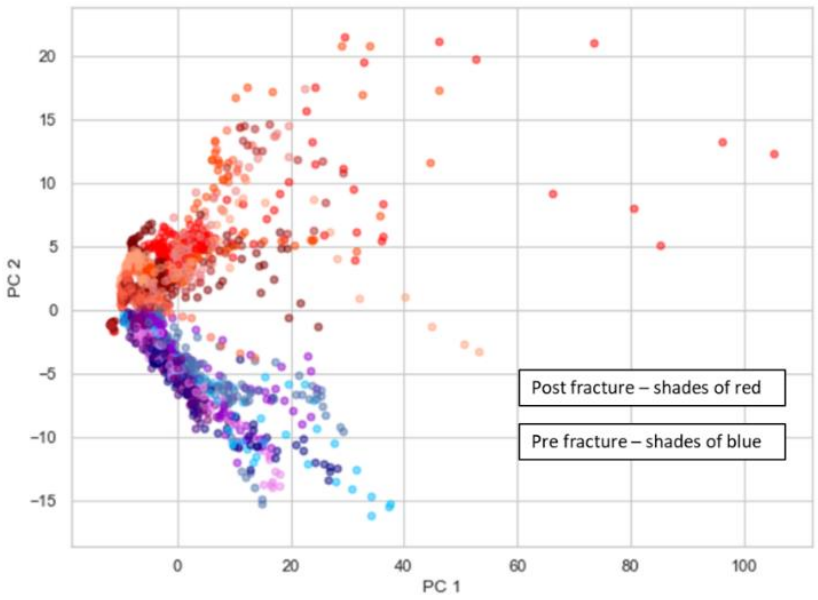

Figure 5: Projection of STFT-derived features from pre-fracture (blue shades) and post-fracture (red shades) in principal component space, projected in first (PC1) and second (PC2) principal components. The difference shades of a color correspond to different transducers. The STFT components of pre- and post-fracture measurements form distinct clusters in PCA space. This is evidence that STFT features in the principal component space can distinguish between shear transmission signals from fractured and intact media.

Unsupervised clustering

Table 2 shows the mean silhouette score for all clusters, for different number of clusters. For the given dataset, K-Means clustering yields the highest silhouette scores. Agglomerative clustering yields slightly lower silhouette scores and is computationally expensive. DBSCAN performs poorly beyond 2 clusters since there are two principal zones of high density, beyond which the efficacy of DBSCAN algorithm falls drastically. Using violin plots (Figure 5), we present the robustness of the clustering results. The violin plot is a method to visualize groups of numerical data exhibiting multimodal distribution. The middle horizontal line in the violin plot marks the median. The horizontal lines at the extremities indicates the 95th percentile of data.

Table 2: Silhouette scores for clustering algorithms considered in this study for sample TSU6

Orientation	Number of Clusters	DBSCAN	K-Means	Agglomerative
Axial	2	0.49	0.55	0.51
	3	-0.15	0.56	0.47
	4	-0.13	0.56	0.52
	5	-0.15	0.29	0.34
	6	-0.17	0.28	0.16
Frontal (fracture perpendicular)	2	-0.25	0.43	0.41
	3	-0.27	0.26	0.24
	4	-0.29	0.25	0.25
	5	-0.29	0.25	0.26
	6	-0.29	0.13	0.11

Frontal (fracture parallel)	2	-0.23	0.75	0.75
	3	-0.30	0.71	0.73
	4	-0.33	0.24	0.22
	5	-0.34	0.26	0.23
	6	-0.34	0.21	0.22

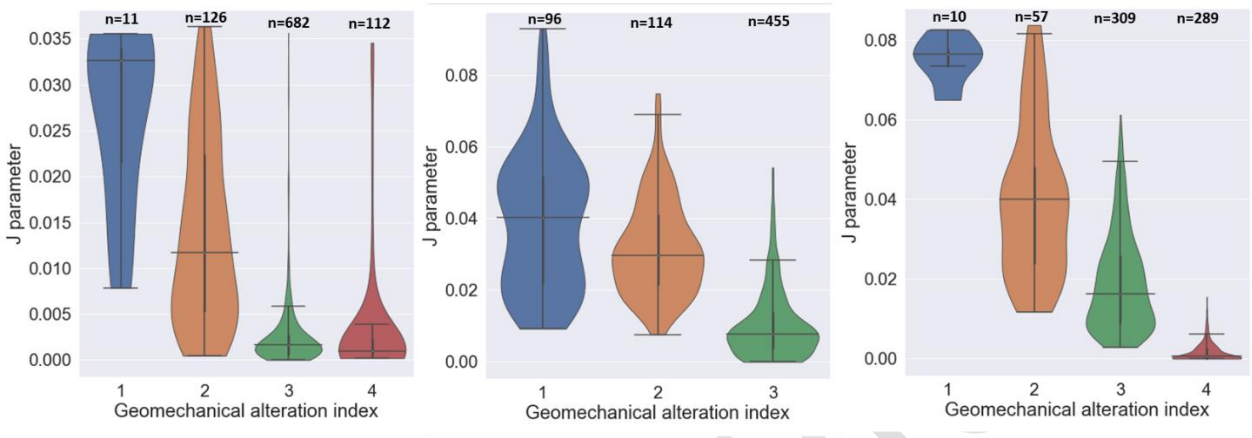

Figure 6: Violin plots of distribution of J parameter (s^{-1}) for axial (left), frontal (fracture perpendicular (middle) and frontal fracture parallel (right) for sample TSU6. 'n' is the number of data points for each cluster.

By jointly considering the difference in the median values of the *J* parameter between different clusters in the violin plots (Figure 6), and the silhouette scores we determined the optimal number of clusters to be 4, 3 and 4 for the axial, frontal (fracture perpendicular) and frontal (fracture parallel) orientations, respectively. Figure 7 shows the output of the workflow for different orientations of the sample TSU6. Hotter colors represent higher geomechanical alteration. In the axial orientation, the damage is localized in the center plane of the sample. The zone of highest GAI coincides with the zone of highest acoustic emission density. In frontal (fracture parallel) orientation, most of the alteration is at the center of the sample. The damage extends towards the lower right of the sample which shows fracture outcrop on the surface. High alteration overlaps the zone of high acoustic emission density. In the frontal (fracture perpendicular) orientation, we note maximum alteration in the upper half of the sample. There is severe alteration in the lower right as well. The damage on the lower right region is not due to fracturing but due to the improper coupling between the sample and the transducers. For the transmitted waves, the improper coupling manifests the same characteristics in the transmitted waves as a fracture. Hence transmitted energy and arrival times at the zones of improper coupling show up as high GAI using the present workflow. As expected, the alteration is high in the regions of high density of acoustic emissions.

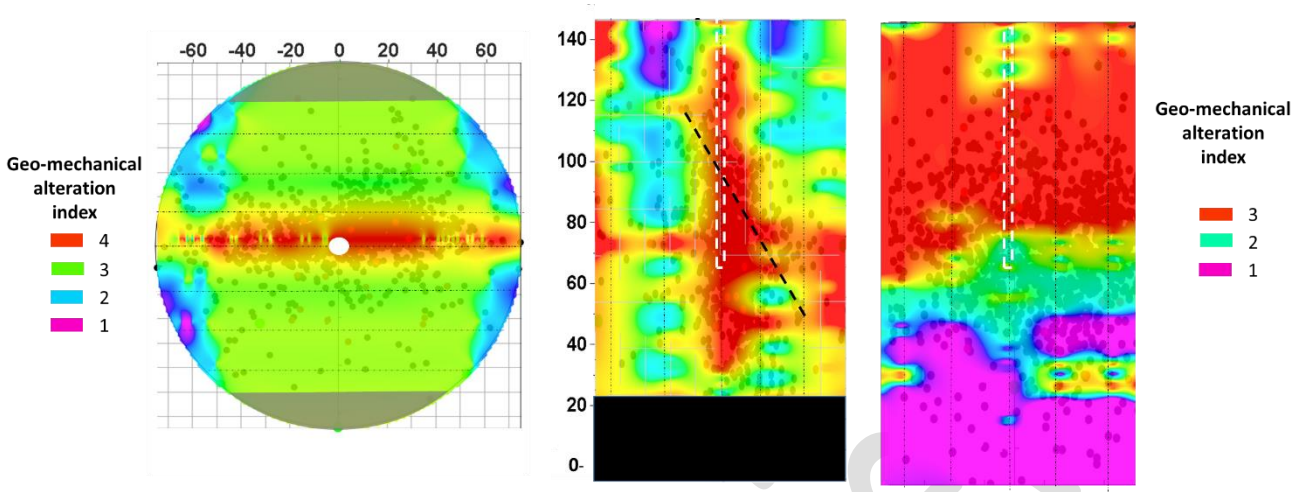

Figure 7: Clustering workflow derived maps of geomechanical alteration index (GAI) for axial (left), frontal perpendicular to fracture (middle) and frontal parallel to fracture (right) orientations for sample TSU6. Grey regions show zones not scanned by transducers, black region indicates region of improper contact between sample and transducers, which may incorrectly appear as high alterations because the mechanical discontinuity due to improper contact will give rise to the same physical changes to the waveform as a fracture/crack in the bulk cylindrical sample. The black dashed line represents the fracture outcrop on the sample. The white dashed rectangle represents the placement of the drilled borehole in the sample. Dots represent the location of acoustic emission hypocenters in the sample recorded during hydraulic fracturing. The distribution of GAI is not parallel to fracture outcrop because of the coarse resolution of the scanning in the direction perpendicular to scanline.

For the sample TSU1, the clustering results of the frontal (fracture parallel) orientation were compared with whole core X-ray CT measurements. In Figure 8 (panel 1) we note as the X-ray slice position moves from position 4 to 1 in the axial plane, the corresponding CT images show the dominant fracture move from the left side of the wellbore to the right. We also note a tapering of the fracture width towards the bottom of the sample (panel 3). However, it does not necessarily imply that the fracture induced damage does not exist towards the sample bottom, instead it indicates that the fracture width at the sample bottom is less than the resolution of the CT. On the corresponding GAI map (Figure 8 (bottom right), the zone of highest GAI is localized in the sample center and extends on both sides of the wellbore. Also, the zone of high alteration appears to taper towards the bottom of the sample, consistent with the X-ray CT measurements.

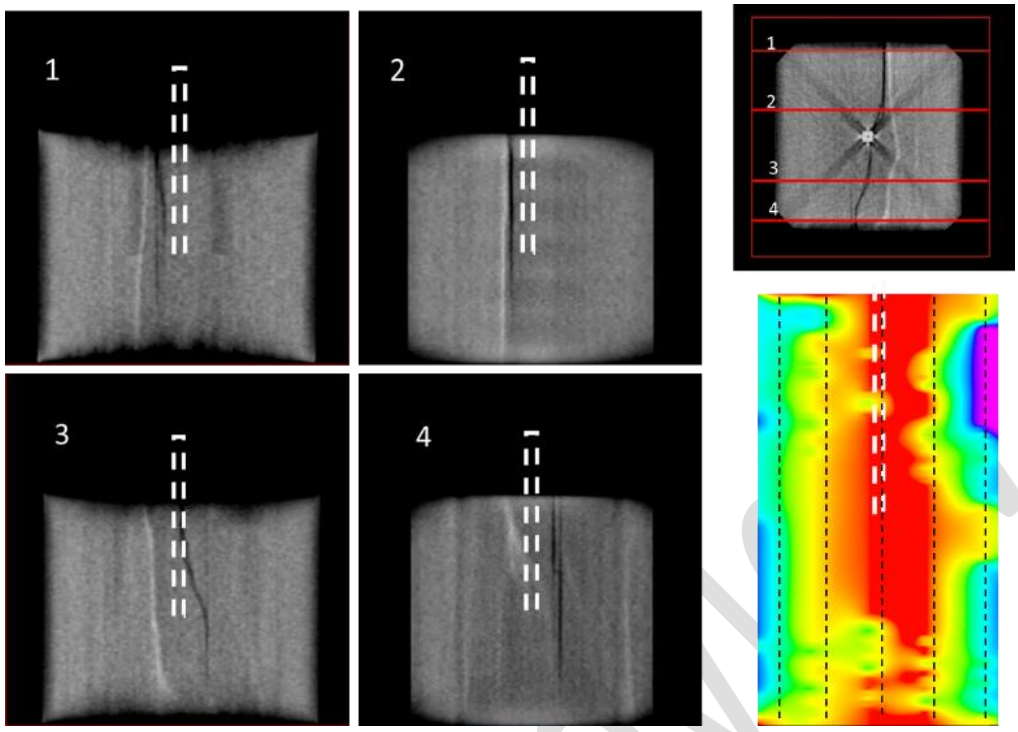

Figure 8: Visualizations of the fracture through X-ray computed tomography for sample TSU1. (upper right) Top view of the sample, red lines show the positions of the four slices within the sample as shown in the left. The four images on the left correspond to the frontal (fracture parallel) orientation. (Lower right) Corresponding map of GAI of the sample.

Assumptions and limitations

The following are the limitations of the present study: (1) the fracture induced alteration can be visualized only in two dimensions, (2) the effects of the presence of the borehole on the ultrasonic wave transmission have been ignored, (3) the effects of sample boundaries on wave propagation have been ignored, and (4) while analyzing transmission data, any zone of improper contact between the sample and transducer will exhibit a high geomechanical alteration index.

Conclusion

In this study, we used data-driven method based on physics-driven unsupervised learning to non-invasively visualize the spatial distribution of geomechanical alteration in geological material induced due to hydraulic fracturing. The workflow preempts the need for picking arrival time of stress waves; thereby, reducing the uncertainty associated with sonic/wave data analysis. The ultrasonic wavelength is of the order of dimension of the mechanical discontinuity. Therefore, the proposed approach does not assume the validity of effective medium theory. Instead, the energy and time-frequency contents of the waveforms are used to cluster the multipoint ultrasonic measurements. Following that, the tenets of the experimentally proven displacement discontinuity theory are applied ascribe physical meaning to the clusters by converting them into a geomechanical alteration index, which proves to be a robust measure of the hydraulic fracturing induced geomechanical alteration. The non-invasive visualizations agree

favorably with acoustic emission and X-ray computed tomography measurements. The use of short-time Fourier transform spectrogram, wave-transmission coefficient, silhouette score based on separation and cohesion, and feature reduction is essential to achieve the desired non-invasive visualization of the geomechanical alteration due to hydraulic fracturing.

For queries contact Dr Sid Misra, Texas A&M University

Acknowledgement

This material is based upon work supported by the U.S. Department of Energy, Office of Science, Office of Basic Energy Sciences, Chemical Sciences Geosciences, and Biosciences Division, under Award Number DE-SC-00019266. We thank the Integrated Core Characterization Center (IC^3) and the Unconventional Shale Gas (USG) Consortium at the University of Oklahoma for providing us the shear waveforms and acoustic emission data.

Declarations

The authors declare that they have no competing interests. AC and SM developed and tested the unsupervised learning and feature extraction methods used in the study. AC and SM prepared the first complete draft of the paper. CR leads the IC3 Lab where PB acquired the data used in the study.

References

[1] E. Majer, J Peterson, T Daley, L Myer, J Queen, P D'Onfro, and W Rizer, "Fracture detection using crosswell and single well surveys". *Geophysics*, vol. 62 no. 2, pp 495–504, Feb. 1997.

[2] D. Burns, M. Willis, M. Toksöz, and L. Vetri. "Fracture Properties from Seismic Scattering", *The Leading Edge*, vol. 26, no. 9, pp 1186-1196, Sep. 2007.

[3] C. Macbeth, "Multicomponent VSP analysis for applied seismic anisotropy". New York, NY, USA: Pergamon, 2002, pp 61-91.

[4] NR. Warpinski, SL Wolhart, and CA Wright, "Analysis and Prediction of Microseismicity Induced by Hydraulic Fracturing", presented at the *SPE Annual Technical Conference and Exhibition,* New Orleans, LA, USA, September 30–October 3, 2001.

[5] S.P. Ojha, S. Yoon, and S. Misra, "Pressure-Transient Responses of Naturally Fractured Reservoirs Modeled Using the Multistencils Fast-Marching Method", *SPE Reservoir Evaluation & Engineering,* vol. 23, no. 1, 2019, pp 112-131, Feb. 2020.

[6] E. H Holley, U. Zimmer, M. J. Mayerhofer, and E. Samson, "Integrated Analysis Combining Microseismic Mapping and Fiber-Optic Distributed Temperature Sensing", presented at the *Canadian Unconventional Resources & International Petroleum Conference*, Calgary, AB, Canada, October 19-21, 2010.

[7] P. Bhoumick, C. Sondergeld, and C. S. Rai, "Mapping Hydraulic Fracture in Pyrophyllite Using Shear Wave", presented at the *U.S. Rock Mechanics/Geomechanics Symposium*, Seattle, WA, USA, June 17-20, 2018.

[8] S. Misra and H. Li, "Noninvasive fracture characterization based on the classification of sonic wave travel times" in *Machine Learning for Subsurface Characterization*. 1st ed. Houston, TX, USA, GPI, 2019, ch.9, sec. 2, pp 243-287.

[9] S Misra, A Chakravarty, P Bhoumick, & C. S Rai, “Unsupervised clustering methods for noninvasive characterization of fracture-induced geomechanical alterations” in *Machine Learning for Subsurface Characterization*. *Machine Learning for Subsurface Characterization*. 1st ed. Houston, TX, USA, GPI, 2019, ch.2, sec. 1, pp 39-64.

[10] A. Damani, A. Sharma, C. H. Sondergeld., and C. S Rai, “Mapping of Hydraulic Fractures under Triaxial Stress Conditions in Laboratory Experiments using Acoustic Emissions”, presented at the *SPE Annual Technical Conference and Exhibition*, San Antonio, TX, USA, October 8-10, 2012.

[11] Y. Wu and S. Misra, “Intelligent Image Segmentation for Organic-Rich Shales Using Random Forest, Wavelet Transform, and Hessian Matrix*”, IEEE Geoscience and Remote Sensing Letters (Early Access)*, Nov. 2019. DOI: 10.1109/LGRS.2019.2943849.

[12] C.J. de Pater, J. Groenenboom, D.B. van Dam, and R. Romijn, “Active seismic monitoring of hydraulic fractures in laboratory experiments”, *International Journal of Rock Mechanics and Mining Sciences*, vol. 38, no. 6, pp 777-785, Aug. 2001.

[13] J. J. S. de Figueiredo, J. Schleicher, R. R. Stewart, N. Dayur, B. Omoboya, R. Wiley, A. William, “Shear wave anisotropy from aligned inclusions: ultrasonic frequency dependence of velocity and attenuation”, *Geophysical Journal International*, vol. 193, no. 1, pp 475–488, Feb. 2013.

[14] LJ Pyrak-Nolte, LR Myer, and NGW Cook, “Transmission of seismic waves across single natural fractures”*, J. Geophys. Res*., vol 95, no. B6, pp 8617– 8638, Jun. 1990.

[15] A Bagheri, K Li, and P. Rizzo, “Reference-free damage detection by means of wavelet transform and empirical mode decomposition applied to Lamb waves”, *Journal of Intelligent Material Systems and Structures,* vol. 24, no. 2, pp 194–208, Sep. 2012.

[16] P.J. Rousseeuw. “Silhouettes: A graphical aid to the interpretation and validation of cluster analysis”, *J. Comput. Appl. Math*, vol. 20, pp 53–65, Nov. 1987.

[17] Everitt, B. S., Landau, S., Leese, M., & Stahl, D. (2011). Cluster analysis: Fifth edition. In *Cluster Analysis: Fifth Edition*. https://doi.org/10.1002/9780470977811